Poleward transport of Eg5 by dynein–dynactin in *Xenopus laevis* egg extract spindles

Marianne Uteng, Christian Hentrich, Kota Miura, Peter Bieling, and Thomas Surrey

Cell Biology and Biophysics Unit, European Molecular Biology Laboratory, 69117 Heidelberg, Germany

Molecular motors are required for spindle assembly and maintenance during cell division. How motors move and interact inside spindles is unknown. Using photoactivation and photobleaching, we measure mitotic motor movement inside a dynamic spindle. We find that dynein–dynactin transports the essential motor Eg5 toward the spindle poles in *Xenopus laevis* egg extract spindles, revealing a direct interplay between two motors of opposite directionality. This transport occurs throughout the spindle except at the very spindle center and at the spindle poles, where Eg5 remains stationary. The variation of Eg5 dynamics with its position in the spindle is indicative of position-dependent functions of this motor protein. Our results suggest that Eg5 drives microtubule flux by antiparallel microtubule sliding in the spindle center, whereas the dynein-dependent concentration of Eg5 outside the spindle center could contribute to parallel microtubule cross-linking. These results emphasize the importance of spatially differentiated functions of motor proteins and contribute to our understanding of spindle organization.

Introduction

The intracellular architecture of eukaryotic cells undergoes drastic changes during the cell cycle. In mitosis, the microtubule cytoskeleton rearranges to form the mitotic spindle, a dynamic, bipolar structure that segregates the duplicated chromosomes to the new daughter cells. How the molecules constituting the spindle organize in space and time is poorly understood. It is clear, however, that the correct spatial arrangement of the spindle components is largely a consequence of the dynamic properties of microtubules and of the forces generated by molecular motors (Wittmann et al., 2001; Gadde and Heald, 2004).

In the spindle, microtubules point with their minus ends toward the spindle poles and with their plus ends to the spindle center (Ding et al., 1993; Mastronarde et al., 1993). Although microtubules are thought to have a mostly uniform orientation close to the poles (Telzer and Haimo, 1981), they overlap in the spindle center in an antiparallel manner (Ding et al., 1993; Mastronarde et al., 1993; Sharp et al., 1999a). Plus ends of spindle microtubules are highly dynamic, switching between phases of growth and shrinkage (Sawin and Mitchison, 1991; Tirnauer et al., 2004), a property called dynamic instability (Mitchison and Kirschner, 1984). In addition, spindle microtubules "flux," with a velocity of ~2 µm/min toward the spindle pole where their minus ends depolymerize (Sawin and Mitchison, 1991; Waterman-Storer et al., 1999). Despite this turnover, the overall appearance of the spindle is stable. To understand such a steady-state system, it is necessary to know the dynamic properties of its components.

Motor proteins transform the chemical energy of ATP hydrolysis into mechanical work (Vale and Milligan, 2000). Two classes of motors interact with microtubules: kinesins (Miki et al., 2005) and dyneins (Oiwa and Sakakibara, 2005). Most but not all kinesins move toward the plus end of microtubules, whereas dyneins step toward the microtubule minus end. Various genetic and biochemical experiments have demonstrated that several members of the kinesin family and cytoplasmic dynein are required for spindle assembly and function (Walczak et al., 1998; Hildebrandt and Hoyt, 2000; Sharp et al., 2000; Goshima and Vale, 2003).

Some of the most important motors for spindle assembly in almost all organisms studied so far are the members of the kinesin-5 (formerly bimC) subfamily. Inhibition or removal of kinesin-5 prevents the formation of bipolar spindles and causes the formation of monopolar structures in higher eukaryotes (Blangy et al., 1995; Mayer et al., 1999; Sharp et al., 1999b; Goshima and Vale, 2003).

Correspondence to Thomas Surrey: surrey@embl.de

Abbreviation used in this paper: biotin-PEG, biotin–polyethylene glycol; CSF, cytostatic factor; paGFP, photoactivatable GFP.

The online version of this paper contains supplemental material.

The Rockefeller University Press $30.00
J. Cell Biol. Vol. 182 No. 4 715–726
www.jcb.org/cgi/doi/10.1083/jcb.200801125

Kinesin-5 motors are homotetrameric (Kashina et al., 1996), plus end–directed (Sawin et al., 1992; Cole et al., 1994; Valentine et al., 2006) molecules, having motor domain dimers at each of the two ends of the elongated molecule (Fig. 1 a). This bivalent arrangement allows members of this kinesin subfamily to cross-link microtubules (Kashina et al., 1996; Sharp et al., 1999a). In spindles, kinesin-5 molecules localize along microtubules, and in vertebrate spindles, are often enriched toward the spindle poles (Hagan and Yanagida, 1992; Sawin et al., 1992; Blangy et al., 1995; Sharp et al., 1999a), a localization that was found to depend on dynein–dynactin (Kapoor and Mitchison, 2001). The main function of Eg5 has mainly been attributed to the sliding of antiparallel microtubules and thus to driving microtubule flux. Sliding of antiparallel microtubules driven by purified Eg5 has been demonstrated directly in vitro (Kapitein et al., 2005), and its importance for microtubule flux in the spindle has been shown by the use of specific inhibitors (Miyamoto et al., 2004). However, exactly how and where in the spindle Eg5 drives microtubule flux is not understood. For example, it has also been proposed that Eg5 is bound to a hypothetical static matrix throughout the spindle (Kapoor and Mitchison, 2001), in which case it could move microtubules relative to this matrix.

To understand the dynamic structure of the spindle, one needs to have a quantitative picture of the dynamic interactions between molecular motors and microtubules under physiological conditions. Despite a wealth of mechanical and biochemical data generated for certain purified motors in vitro (Cross, 2004), there is hardly any information available about the local activities of motors in their physiological context. Here, we measured the movement of Eg5 relative to the movement of microtubules inside *Xenopus laevis* egg extract spindles using time-lapse fluorescence microscopy in combination with photoactivation (Lippincott-Schwartz et al., 2003) and photobleaching (Sprague and McNally, 2005). We found that the dynamic behavior of Eg5 varied with its position along the spindle axis. In the region of antiparallel microtubule overlap in the spindle center, Eg5 was stationary relative to the spindle axis. Outside of the central antiparallel microtubule overlap, however, we observed poleward movements of Eg5. These movements were dependent on the interaction of Eg5 with a functional dynein–dynactin complex.

Results

Eg5 fused to photoactivatable GFP (paGFP) is functional in organizing microtubules in buffer and in *X. laevis* egg extract

We generated a recombinant construct of *X. laevis* Eg5 fused to paGFP (Eg5-paGFP) to be able to follow the movements of this motor inside mitotic spindles. We confirmed the functionality of this construct using two assays.

First, we tested the ability of purified Eg5-paGFP to slide antiparallel microtubules in buffer. We created microtubule pairs connected by Eg5 in which one microtubule of each pair was selectively immobilized on a chemically functionalized glass surface (see Materials and methods), whereas the other microtubule was free to move (Fig. 1 a). Nonspecific adsorption of Eg5 to the surface was prevented by a dense polyethylene glycol layer covalently bound to the glass, ensuring that microtubule movement occurred only between microtubule pairs. This assay allowed us to create a large number of microtubule pairs that we observed by fluorescence microscopy (Fig. 1 b). Although about half of the generated pairs were static, which is indicative of parallel microtubule orientation, the other half contained a microtubule that was translocated by Eg5, which is indicative of an antiparallel pair (Kapitein et al., 2005). Sliding velocity distributions could be determined reliably from the movements of microtubules in antiparallel pairs (Fig. 1 c). Microtubules driven by purified Eg5 without a paGFP tag moved with a mean velocity of 2.8 ± 0.7 μm/min relative to immobilized microtubules (Fig. 1 d). This velocity agrees with results from a previous study (Kapitein et al., 2005) and is very similar to the 3.3 ± 0.7 μm/min measured for Eg5-paGFP (Fig. 1 d). This indicates that paGFP in the fusion protein has no deleterious influence on the motile properties of Eg5 in buffer.

We next replaced native Eg5 by Eg5-paGFP (Kapoor and Mitchison, 2001) in *X. laevis* egg extract by adding recombinant Eg5-paGFP to immunodepleted extract at concentrations corresponding to the previously described endogenous level (Kapoor and Mitchison, 2001). Eg5-paGFP rescued spindle formation and localized to the spindle as described previously (Fig. S1, available at http://www.jcb.org/cgi/content/full/jcb.200801125/DC1; Sawin et al., 1992; Kapoor and Mitchison, 2001). This demonstrated that Eg5-paGFP is also functional in *X. laevis* egg extracts. We were therefore in a position to measure the dynamics of Eg5 in *X. laevis* egg extract spindles in which the entire Eg5 pool was tagged with paGFP, and to compare the movements of Eg5 in the spindle with its behavior in buffer using the same Eg5 construct.

Local dynamics of Eg5 in different positions of the spindle measured by fluorescence loss after photoactivation

We next measured the dynamic behavior of Eg5 and of microtubules in *X. laevis* egg extract spindles that were assembled in Eg5-depleted, cycled extracts supplemented with recombinant Eg5-paGFP and with fluorescently labeled tubulin. We recorded time lapse videos with confocal fluorescence microscopy after simultaneous photoactivation of Eg5-paGFP and photobleaching of Cy5-tubulin in various regions in the spindle. We photoactivated and photobleached stripes of a 3-μm width perpendicular to the spindle axis in up to three different spindle regions: (1) in the spindle center, i.e., the "midzone"; (2) at the poles; and (3) in the region between midzone and pole that we call here the "halfzone" (Fig. 2). These measurements yield the temporal development of ensembles of locally photoactivated Eg5-paGFP molecules and of locally bleached Cy5-microtubules (Figs. 3 a and S2 a; and Videos 1–3, available at http://www.jcb.org/cgi/content/full/jcb.200801125/DC1). The measured fluorescence intensities of photoactivated Eg5-paGFP and of Cy5 microtubules at the different time points were then projected onto the pole-to-pole axis of the spindles, creating one-dimensional fluorescence intensity profiles along the spindle axis (Fig. 2). From these intensity profiles, mean velocities of movement and mean

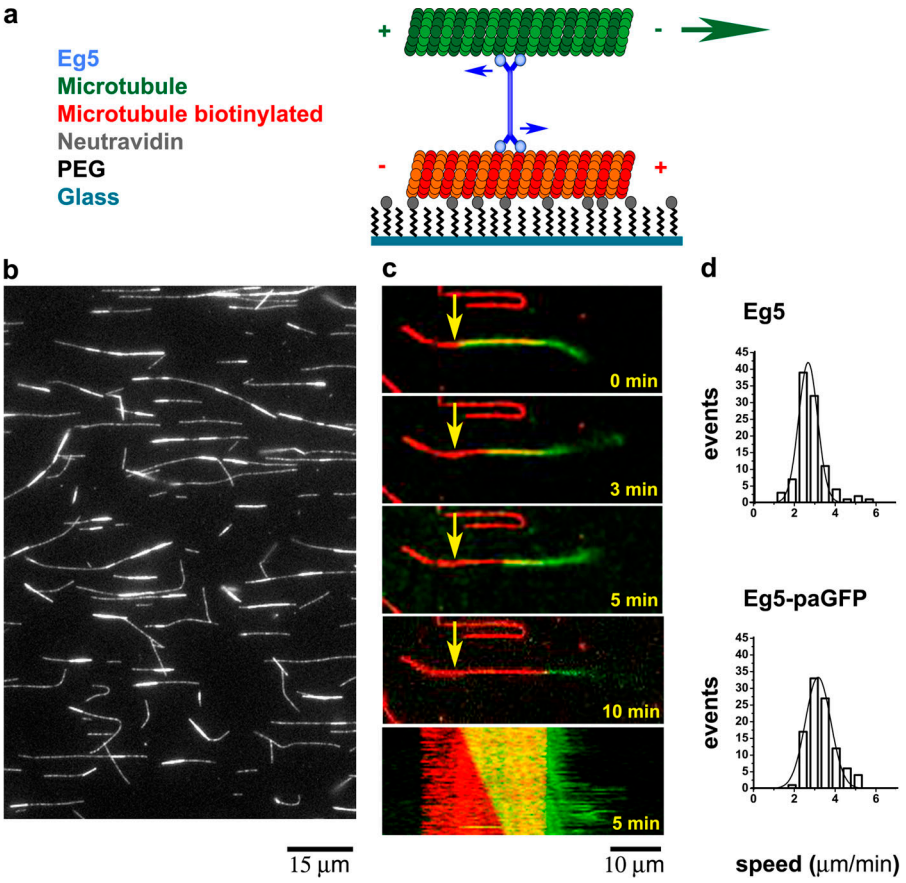

Figure 1. **Microtubule pair sliding driven by purified Eg5 in buffer.** (a) Schematic of Eg5 within a pair of antiparallel microtubules. The red microtubule is biotinylated and immobilized to a chemically functionalized glass surface via biotin–neutravidin links. The green microtubule is not biotinylated and mobile. (b) Fluorescence microscopy images of Alexa 568 microtubule pairs formed with Eg5-paGFP. Dimly labeled microtubules immobilized on a biotin-PEG glass surface supporting Eg5-mediated binding of brightly labeled microtubules (see Materials and methods). (c) Time series of confocal fluorescence microscopy images of a Cy5-labeled microtubule (green) moved by Eg5 along an immobilized Alexa 568–labeled microtubule (red). Arrows indicate the initial position of the Cy5-labeled microtubule. The bottom panel shows a kymograph of a line along the microtubule pair during the first 5 min of the time series. (d) Histograms showing distributions for speeds of microtubule sliding driven by Eg5 and Eg5-paGFP.

turnover rates of photoactivated Eg5 and photobleached microtubules were extracted for the different regions in the spindle (see Materials and methods). To be able to compare the positions of the minima of the fluorescence intensity profiles of Cy5-tubulin with the maxima of the intensity profiles of Eg5-paGFP, we created "inverted" intensity difference profiles for Cy5-tubulin by subtracting the postbleach profiles from its last prebleach profile (Fig. 2 and Materials and methods). By analyzing the displacement of these peak maxima, with time, we obtained the velocities of microtubule flux and of the photoactivated Eg5 pool in the spindle. Furthermore, as the measurement of both Eg5 and Cy5-tubulin was performed simultaneously within the same spindle, we could also analyze the movement of Eg5 relative to the movement of microtubule flux.

Eg5 movements vary with the position in the spindle

We observed different behaviors of Eg5 depending on its position in the spindle. Although Eg5 appeared stationary in the spindle center (Kapoor and Mitchison, 2001), surprisingly, it moved toward the spindle poles in the halfzone (Fig. 3 a).

In the spindle midzone, the inverted Cy5-tubulin profiles did not only decrease with time as a consequence of tubulin turnover, but the peak also broadened and split into two peaks after ~30 s (Fig. 3 b). This is in agreement with earlier observations and a consequence of the sliding of antiparallel microtubules into opposite directions in the spindle midzone (Sawin and Mitchison, 1991; Miyamoto et al., 2004). In the example shown, velocities of −3.4 μm/min toward one pole and of 1.5 μm/min toward the other pole of the spindle were obtained from plots of the position of the peak maxima versus time (Fig. 3 c). In contrast to the microtubule photobleach mark, the fluorescence signal of photoactivated Eg5-paGFP did not split, and the position of its maximum stayed in the middle of the two splitting microtubule peaks (Fig. 3 b). Consequently, the position of the maximum of the Eg5 intensity profile moved only slightly in this example, with a velocity of 0.6 μm/min in the direction of the faster-moving microtubule signal (Fig. 3 c). The slight asymmetry of movement in the spindle shown here is probably a consequence of having illuminated the spindle not exactly in its center. The mean velocity of Eg5 determined in the midzone of four spindles was 0.05 ± 0.59 μm/min. This result indicates that Eg5 cross-links and pushes microtubules toward the poles while remaining stationary in the center of the spindle.

The dynamic behavior of Eg5 and microtubules was strikingly different in the halfzone as compared with the midzone of the spindle. As expected, the photobleached microtubule region moved unidirectionally toward the spindle pole (Fig. 3, a and b). This is in agreement with the notion that microtubules are mostly parallel in this region of the spindle (Telzer and Haimo, 1981) and that they flux toward the poles (Sawin and Mitchison, 1991; Miyamoto et al., 2004). Interestingly, the fluorescent pool of photoactivated Eg5 in the halfzone also moved toward the pole (Fig. 3, a and b). The velocity of this movement of Eg5 was faster than the microtubule flux (Fig. 3 c). On average, the poleward speed of Eg5 was 2.8 ± 0.9 μm/min, a speed significantly faster than the

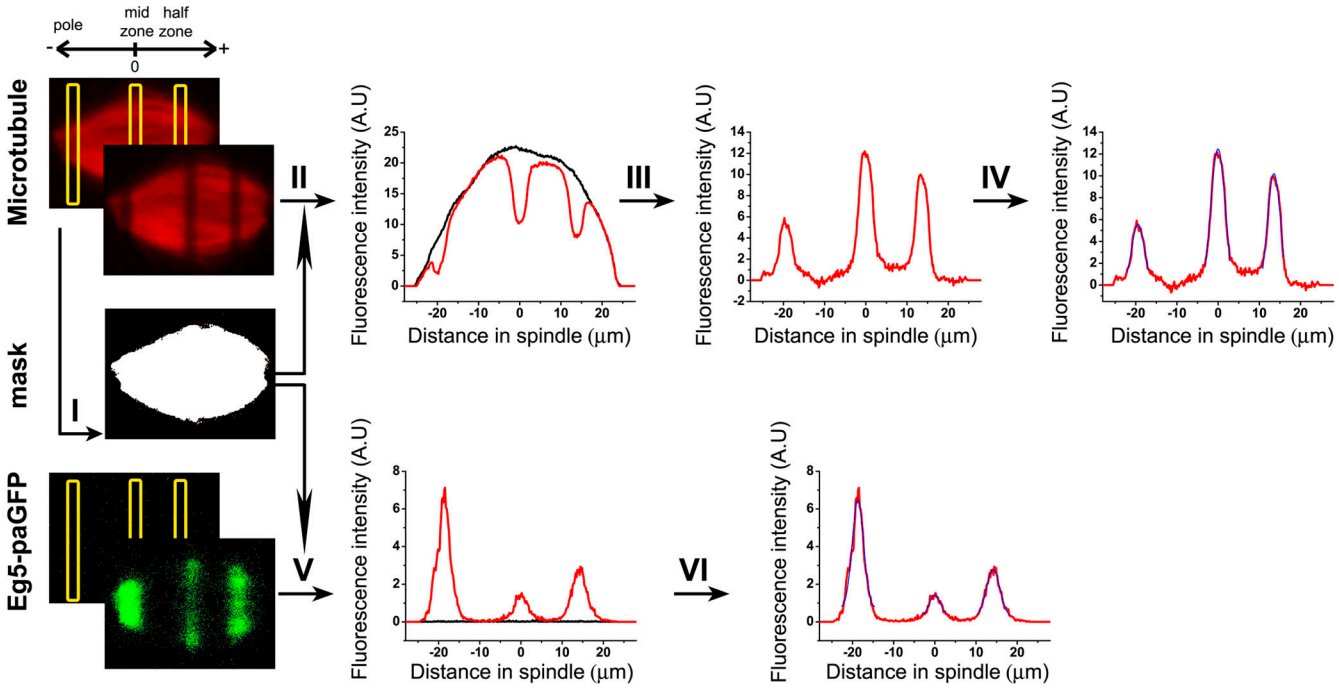

Figure 2. **Fluorescence intensity profiles from spindles after photobleaching and photoactivation.** Time-lapse videos of a confocal section through spindles containing Cy5 microtubules and photoactivatable Eg5-paGFP were recorded simultaneously in the Cy5 and GFP channel of a confocal fluorescence microscope. Between the first and the second image of a time series, one or several rectangular stripes in the confocal section were bleached and simultaneously photoactivated. To convert the images of the two time series into fluorescence intensity profiles, the area of the spindle in the Cy5 microtubule image before the photobleach was determined by applying an intensity threshold to the image (I). This area served then as a mask for the entire time series of the Cy5 microtubule images and the Eg5-paGFP (illustrated here only for the second frame of the time series). The intensity values were projected onto the spindle axis. This created fluorescence intensity profiles (II and V). The turnover of microtubules and of Eg5 was extracted from time series of these intensity profiles (II and V; see Materials and methods). To determine the exact position of the maximum amount of bleached microtubules, the Cy5 intensity profiles were subtracted from the prebleach profile, resulting in an inverted intensity difference profile (III). The positions of the maximum of the intensity difference profiles of Cy5 microtubules and of the intensity profiles of photoactivated Eg5-paGFP were determined from a Gaussian fit (blue) to the profiles (IV and VI) and used to calculate the velocity of the movements of the peaks (see Materials and methods).

mean speed of microtubule flux that was 1.5 ± 0.6 µm/min (Fig. 3 d; P = 0.00005, Mann-Whitney *U* test with significance level of 0.05). In control experiments, we demonstrated that such a statistically significant difference is also obtained if Eg5 velocities are compared with microtubule flux measured by speckle microscopy (Fig. S3, available at http://www.jcb.org/cgi/content/full/jcb.200801125/DC1), which indicates that this result is independent of the method used. We draw two conclusions from these results. First, in well-focused spindles, the plus end–directed motor Eg5 is transported toward the minus ends of microtubules. Second, microtubule flux is not sufficient to explain this transport, which suggests the existence of an additional minus end–directed transport mechanism. At the pole of the spindle, no or only little movement along the spindle axis was observed for photobleached microtubules or photoactivated Eg5 (Fig. 3, b and c). In conclusion, Eg5 is not static but dynamic in the *X. laevis* egg extract spindle, and its movements vary in a characteristic manner with its position along the spindle axis.

The turnover of Eg5 varies with the position in the spindle

To extract information about the turnover of Eg5 and tubulin from our photoactivation and photobleaching experiments, we followed the overall intensity of the moving photoactivated pool of Eg5-paGFP and of the moving photobleached pool of Cy5-tubulin over time (see Materials and methods). Consequently, the measurement of the changing overall intensity was not influenced by the movement of the photoactivated or photobleached pools (see Materials and methods). This separated the analysis of binding/unbinding turnover from that of movement. The decays of the Eg5 fluorescence were approximately exponential during an initial period of 2 min (Fig. 4 a), and this period was used for the analysis. The mean half-life of Eg5 in the spindle was generally either shorter or in the same range of the mean half-life of tubulin, with the exception of the poles (Fig. 4 a). The mean half-life of Eg5 increased significantly from 25 ± 6 s in the midzone to 71 ± 39 s at the pole (Fig. 4 b; P = 0.006, Mann-Whitney *U* test with a significance level of 0.05). The monoexponential fits lead also to the detection of a residual spindle-associated pool of Eg5 that was dissociating more slowly from the spindle, as became evident when observing the turnover for longer periods of time (up to 5 min). Bleaching during observation of turnover did not affect the measured rates as could be demonstrated in control experiments (Fig. S2 b and Materials and methods).

Loss of dynein–dynactin drastically reduces the amount of Eg5 in *X. laevis* egg extract spindles

To test if Eg5 is transported in the halfzone by the minus end–directed motor dynein–dynactin (Schroer, 2004; Oiwa and

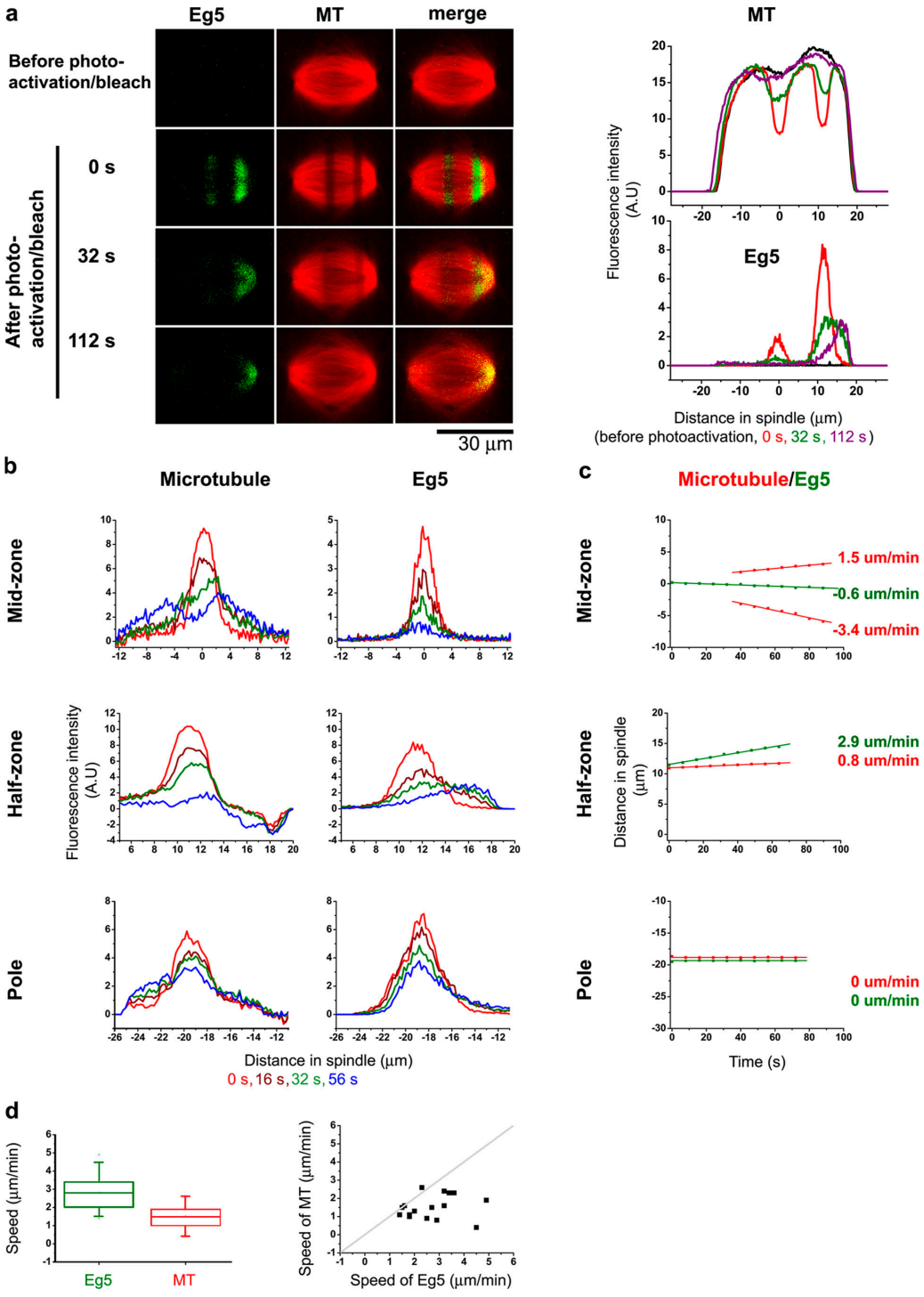

Figure 3. **Directed movements of photoactivated Eg5-paGFP and of photobleached Cy5 microtubules along the spindle axis.** (a) Spindles in egg extract depleted from endogenous Eg5 and supplemented with Eg5-paGFP and Cy5-tubulin before and after photoactivation of Eg5-paGFP and simultaneous photobleaching of Cy5 microtubules in two different spindle regions. Time series of confocal fluorescence microscopy images of Eg5-paGFP (green) and Cy5 microtubules (MT; red) at the indicated times, and fluorescence intensity profiles (Fig. 2) for Cy5 microtubules and Eg5-paGFP of the same spindle at the indicated times. (b) Intensity difference profiles for bleached Cy5 microtubules and intensity profiles for photoactivated Eg5-paGFP at the indicated times. Only parts of entire profiles are shown for the midzone, halfzone, and pole region. Intensity difference profiles for Cy5 microtubules appear inverted as compared with the intensity profiles (Fig. 2). Note the splitting of the initial single peak of the red microtubule profile in the midzone into two peaks of the blue microtubule profile after 56 s. A corresponding split is not observed in the Eg5 profiles. The intensity profile for the halfzone is derived from the spindle shown in section a, whereas the intensity profiles for the midzone and pole are derived from spindles not shown because of different imaging requirements for the different regions in the spindle. (c) Displacements of the peaks of photoactivated Eg5-paGFP (green) and of photobleached Cy5 microtubules (red) along the spindle axis with time. Linear regression fits (lines) to the experimental values (dots) yielded the velocities as indicated. (d, left) Box plots of the speeds of Eg5 movement (22 measurements in 19 spindles) and of microtubule flux (MT; 16 measurements). (right) Scatter diagram of the speeds of microtubule (MT) flux as a function of the speeds of Eg5 in the halfzone. Each data point represents two simultaneous measurements in the same spindle region.

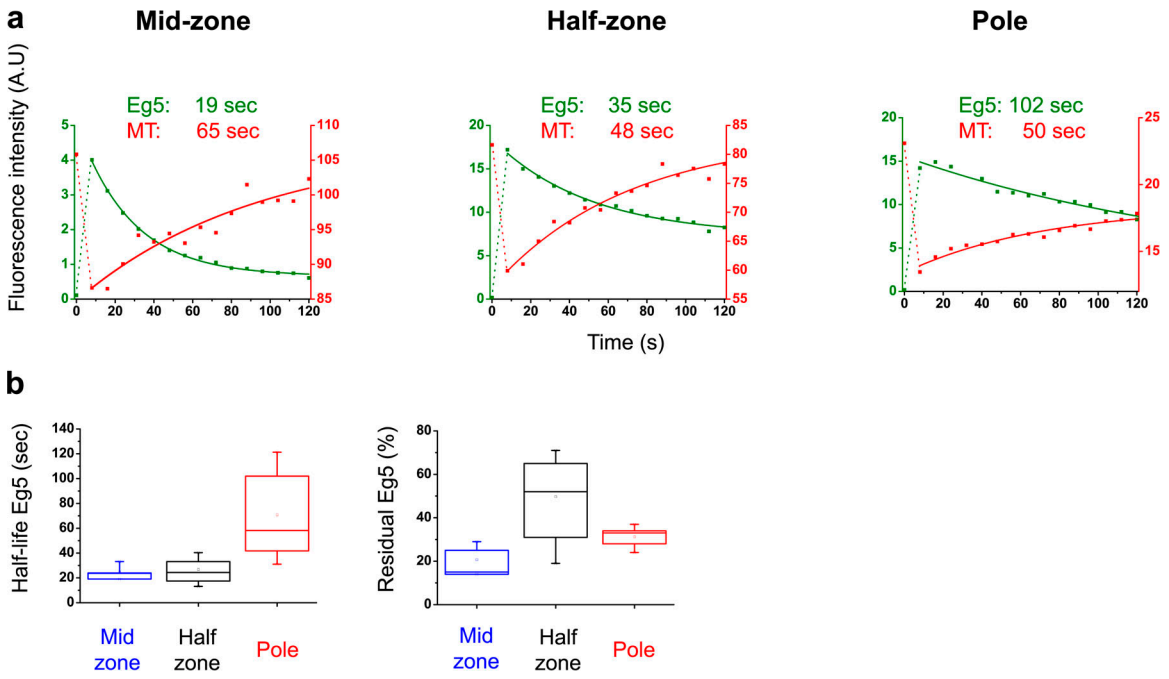

Figure 4. **Turnover of Eg5 and microtubules in egg extract spindles measured by time-lapse fluorescence microscopy after photoactivation and photobleaching.** (a) Fluorescence decay of photoactivated Eg5-paGFP (green) and fluorescence recovery of Cy5 microtubules (red) in the midzone, the halfzone, and the pole region within the first 2 min after photoactivation and photobleaching. A monoexponential fit (lines) to the experimental values (dots) yielded half-lives as indicated. (b) Box plots of half-lives and residuals of fluorescence decays of photoactivated Eg5-paGFP in the three different spindle regions. 4–12 measurements were made per region.

Sakakibara, 2005), we disrupted the dynein–dynactin complex by the addition of human p50 (dynamitin) (Wittmann and Hyman, 1999; Melkonian et al., 2007) or of a fragment containing the first coiled coil (cc1) of *X. laevis* p150^{Glued} (King et al., 2003; Gaetz and Kapoor, 2004), which is part of the dynactin complex. It is known that under these conditions, spindles form with pole and length defects (Fig. 5 a). Monitoring the fluorescence intensity of photoactivated Eg5-paGFP, we found that in addition to the previously described redistribution of Eg5 in *X. laevis* egg extract spindles (Kapoor and Mitchison, 2001), the total amount of Eg5 in spindles with disrupted dynein–dynactin complexes was drastically reduced as compared with unperturbed spindles (Fig. 5, a and b). The amount of Eg5 per spindle tubulin decreased to only 26 and 15% (as compared with control spindles) in extracts treated with p50 and cc1, respectively (Fig. 5 b). The most drastic reductions of Eg5 amount were observed in the halfzone and at the poles.

Interestingly, the typical localization of dynein–dynactin to spindle microtubules and its enrichment toward the spindle poles (Heald et al., 1997) is also lost upon disruption of the dynein–dynactin complex (Figs. 5 c and S4, available at http://www.jcb.org/cgi/content/full/jcb.200801125/DC1). Using pull-down assays, we could furthermore show that in *X. laevis* egg extract, Eg5 interacts biochemically with p150^{Glued} (Fig. 5 d), an interaction previously detected in a yeast two-hybrid screen (Blangy et al., 1997). This interaction was detected also in the presence of nocodazole, demonstrating that it was not mediated via microtubules. Furthermore, we were able to disrupt this biochemical interaction between Eg5 and p150^{Glued} upon addition of cc1 to the extract, demonstrating the specificity of this interaction (Fig. 5 d). Collectively, these results suggest that movement and accumulation of Eg5 toward the spindle poles is a consequence of its interaction with dynein–dynactin.

Transport of Eg5 toward the spindle pole by dynein–dynactin

To test the consequences of the reduction of the amount of dynein–dynactin from spindle microtubules upon dynactin disruption on the dynamics of Eg5 at different positions in the spindle, we performed photoactivation and photobleaching experiments in spindles reconstituted in extract supplemented with either p50 or cc1.

In the midzone of p50 spindles, the behavior of Eg5-paGFP and Cy5-microtubules was similar to that in the midzone of wild-type spindles. Overlapping microtubules moved to opposite ends of the spindles, as indicated by a splitting microtubule bleach mark, whereas the signal of photoactivated Eg5 decayed without splitting (Fig. 6 a). In the halfzone of the perturbed spindles (Fig. 6, b and c), the mean speed of microtubule flux was 2.5 ± 0.5 µm/min and 1.7 ± 0.7 µm/min for p50 and cc1 spindles, respectively (Fig. 6, d and e). The movement of Eg5-paGFP in the halfzone of the perturbed spindles was now strikingly slower than in wild-type spindles (Fig. 6, d and e). Eg5 moved toward the poles with a mean speed of 1.0 ± 0.8 µm/min and 0.6 ± 0.7 µm/min in p50 and cc1 spindles, respectively, now moving significantly more slowly than the fluxing microtubules (Fig. 6, c–e; p50 spindles, P = 0.0001; cc1 spindles, 0.0001; Mann-Whitney *U* test with significance level of 0.05). These results suggest that Eg5 is able to step toward the spindle midzone along microtubules that flux into the opposite direction, resulting

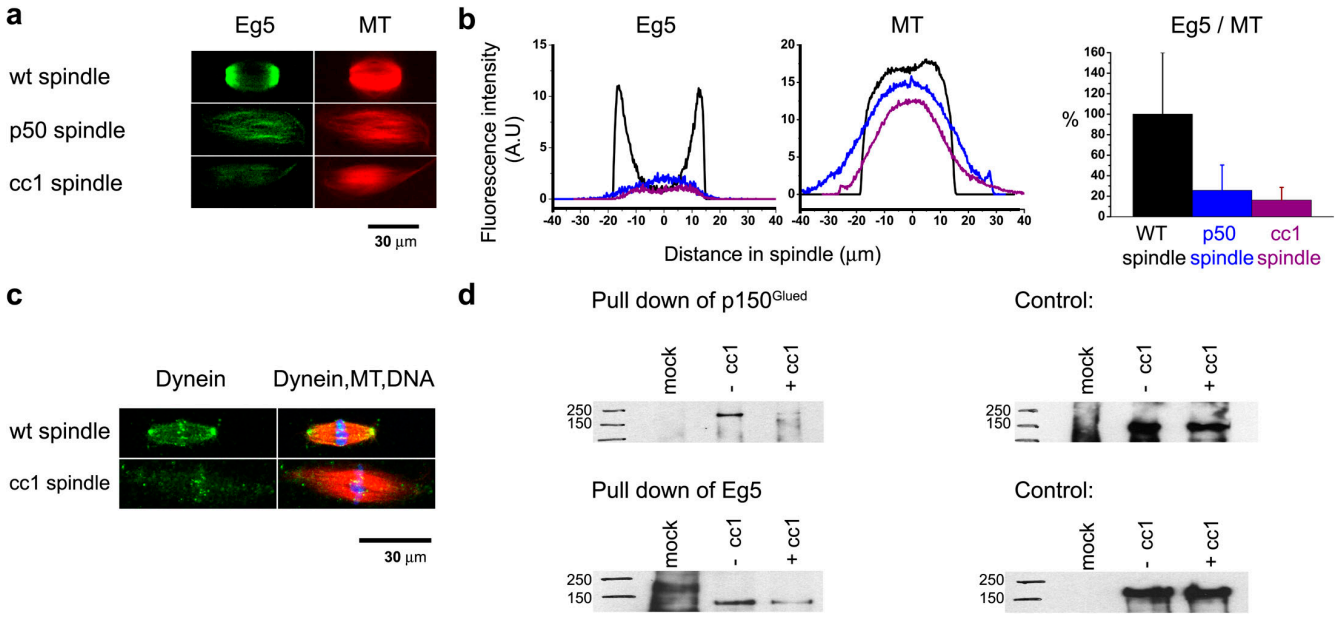

Figure 5. **Disruption of the dynein–dynactin complex decreases the amount of Eg5 localizing to spindles in *X. laevis* egg extract.** (a) Confocal fluorescence microscopy images of nonfixed spindles assembled either in the absence or additional presence of p50 or cc1 showing the localization of Eg5. The fluorescence of Eg5-paGFP (green) and of Cy5 microtubules (MT; red) was measured immediately after photoactivation of Eg5-paGFP in the entire spindle. (b) Fluorescence intensity profiles for photoactivated Eg5-paGFP and Cy5 microtubules along the spindle axis for the spindles shown in section a. (right) Mean ratios of the total fluorescence intensity of photoactivated Eg5-paGFP divided by the total fluorescence intensity of Cy5 microtubules (MT) for wild-type spindles, p50 spindles, and cc1 spindles are shown. The means were determined from five spindles per condition. The wild-type intensity ratio was set to 100. Error bars indicate standard deviation. (c) Confocal fluorescence microscopy images of fixed spindles assembled either in the absence (top) or presence (bottom) of cc1 showing the localization of dynein. Dynein heavy chain was detected by immunofluorescence (green), tubulin by using incorporated Alexa 568–tubulin (red), and DNA by Hoechst staining (blue). (d) Western blot analysis showing pull-down of $p150^{Glued}$ with Eg5 on anti-Eg5 beads and pull-down of Eg5 with $p150^{Glued}$ on anti-$p150^{Glued}$ beads in *X. laevis* egg extract, either in the absence (−cc1) or presence (+cc1) of added p150 fragment cc1. Mock represents magnetic beads coated with an irrelevant antibody also incubated in *X. laevis* egg extract. An anti-$p150^{Glued}$ antibody was used for detection in the top left three lanes and in the bottom right three lanes, whereas an anti-Eg5 antibody was used for detection in the top right three lanes and in the bottom left three lanes. All samples in a horizontal row were run on the same SDS gel. Molecular weight markers to the left of the blots are in kD.

in only a slow net movement of Eg5 toward the pole. Interestingly, in some cases, the photoactivated pool of Eg5-paGFP moved even toward the spindle center (negative speed values in Fig. 6, d and e), which indicates that Eg5 now steps even faster toward the microtubule plus end than the microtubules move toward the poles. We conclude from these results that in wild-type spindles, the dynein–dynactin complex is responsible for transport of Eg5 toward the poles.

The turnover of Eg5 in p50 and cc1 spindles was not significantly different from the turnover in the halfzone of unperturbed spindles (Fig. 6 f; wild type vs. p50 spindles, $P = 0.39$; wild type vs. cc1 spindles, $P = 0.19$; Mann-Whitney U test with significance level of 0.05). We did also not observe a variation of the turnover of Eg5 with position along the spindle axis in these perturbed spindles. This is probably caused by the absence of intact spindle poles in these spindles.

We finally tested if transport of Eg5 by dynein–dynactin was mediated by the charged part of the C-terminal tail of the Eg5 molecule. We created a mutant of Eg5 in which the last 76 C-terminal amino acids were removed, without disrupting the conserved Cdk1 site at position 937. We found that the truncated Eg5 construct behaved very similarly to wild-type Eg5, both in buffer and in egg extract (Fig. S5, available at http://www.jcb.org/cgi/content/full/jcb.200801125/DC1). Thus, the C-terminal part of the Eg5 tail is neither important for dynein-dependent transport of Eg5 in the spindle nor for spindle formation.

Discussion

We performed simultaneous measurements of the dynamic behavior of photoactivatable Eg5 and of microtubules in *X. laevis* egg extract spindles. We measured these dynamics at different positions of the spindle in the presence and absence of an intact dynein–dynactin complex. Our measurements suggest a model with different functions of Eg5 depending on its position in the spindle.

In the midzone, where antiparallel microtubules overlap (Mastronarde et al., 1993), Eg5 cross-links antiparallel microtubules (Sharp et al., 1999a) and slides them apart (Miyamoto et al., 2004), similar to its action between antiparallel microtubule pairs in buffer (Fig. 1; Kapitein et al., 2005). Consequently, photoactivated Eg5 remained stationary in the spindle center, whereas microtubules were pushed to opposite poles of the spindle (Fig. 3). We found that the speed with which antiparallel microtubules move apart from each other in the spindle center (twice the speed of flux) is similar to the speed of antiparallel microtubule sliding measured with the same photoactivatable Eg5 construct in buffer. Thus, these results suggest that Eg5 slides overlapping microtubules with its intrinsic biophysical properties in the spindle center. Interestingly, flux of kinetochore microtubules was found to be independent of Eg5 function in mammalian cells (Cameron et al., 2006). This agrees with the proposal that Eg5 drives flux of those microtubules that overlap in the spindle center in an antiparallel manner.

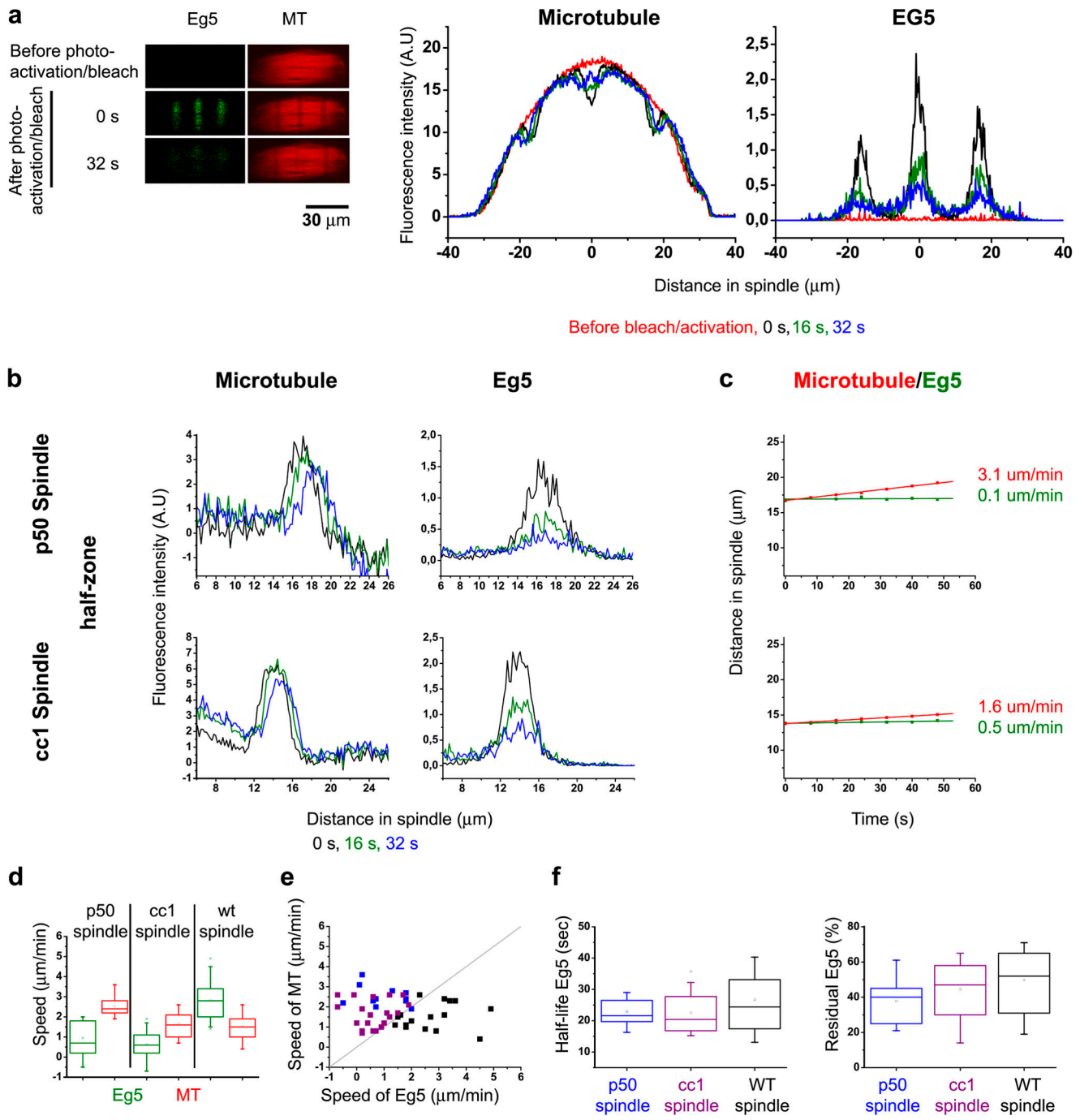

Figure 6. **Dynamics of Eg5 and microtubules in spindles assembled after disruption of the dynein–dynactin complex.** (a) Spindle assembled in the presence of p50. Confocal fluorescence microscopy images of photoactivated Eg5-paGFP (green) and Cy5-labeled microtubules (red) before and after photoactivation and simultaneous photobleaching in three different spindle regions. Fluorescence intensity profiles for Eg5-paGFP and Cy5 microtubules (MT) of the same spindle at the indicated times. (b) Sections of intensity difference profiles for bleached Cy5 microtubules and intensity profiles for photoactivated Eg5-paGFP in the halfzone of spindles assembled in the presence of p50 or cc1. (c) Displacements of the peaks of photoactivated Eg5-paGFP (green) and of photobleached Cy5 microtubules (red) along the spindle axis with time. Linear regression fits (lines) to the experimental values (dots) yielded the velocities as indicated. (d) Box plots of the speeds of Eg5 and of microtubule flux (MT) in the halfzone of p50 spindles (11 measurements in 6 spindles) and cc1 spindles (20 measurements in 11 spindles) as compared with wild-type spindles (data from Fig. 3 d). (e) Scatter diagram of speeds of directed movements of photoactivated Eg5-paGFP in the halfzone of p50 spindles (blue), cc1 spindles (green), and in unperturbed spindles (black) as a function of the simultaneously measured speeds of microtubule (MT) flux. (f) Box plots of the half-lives of the fluorescence decays of photoactivated Eg5-paGFP in p50 spindles, cc1 spindles, and unperturbed spindles (data from Fig. 4 b) and box plots of the corresponding residuals. Shown are the same measurements as in section e.

In the halfzone, where the majority of microtubules are thought to have a parallel orientation with their minus ends oriented toward the pole (Telzer and Haimo, 1981; McIntosh and Euteneuer, 1984; Ding et al., 1993; Mastronarde et al., 1993), Eg5 was observed to move toward the spindle poles with a speed clearly faster than microtubule flux (Fig. 3). Such a poleward

movement is the opposite of what one would expect from a plus end–directed motor like Eg5. One may speculate that this movement could derive from an indirect effect of dynein–dynactin on Eg5 movements. For instance, Eg5 could be bound to short microtubules that in turn could be transported by dynein–dynactin toward the poles. Indeed, recent experiments suggested that the majority of the microtubules in *X. laevis* egg extract spindles are significantly shorter than the pole-to-chromosome distance (Burbank et al., 2006, 2007; Yang et al., 2007) and that a certain heterogeneity of flux velocities exists in the tiled array of short microtubules (Yang et al., 2007). However, unless Eg5 binds selectively to the subset of fast microtubules, this scenario of indirect transport of Eg5 by microtubules is unlikely. Instead, our data suggest that Eg5 is transported by dynein–dynactin in a more direct manner, as we could demonstrate a biochemical interaction between Eg5 and the dynactin subunit $p150^{Glued}$ in egg extract. Our data do not, therefore, support a model in which Eg5 is bound to a hypothetical static matrix throughout the spindle (Kapoor and Mitchison, 2001), but rather show that Eg5 is undergoing poleward movement in the spindle halfzone as a consequence of dynein–dynactin transport.

What is the function of poleward transport of Eg5 in the spindle? The velocity of the poleward transport of Eg5 was significantly slower than the velocity of purified dynein in buffer (King and Schroer, 2000). This may indicate that Eg5 still interacts with microtubules when being transported by dynein, effectively causing a tug of war between these two motors in which dynein dominates, although suffering a significant slowdown as compared with its speed in the absence of a hindering load. The notion that Eg5 can still interact with microtubules in the halfzone is supported by our observation that after disrupting its interaction with $p150^{Glued}$, the movement toward the pole was drastically reduced, or even sometimes reversed toward the spindle center. This result indicates that Eg5 located in the halfzone of the spindle can move with its intrinsic activity toward microtubule plus ends that are oriented toward the spindle center. Thus, the function of the poleward accumulation of Eg5 could be to contribute to microtubule bundling or even clustering of microtubules by connecting parallel microtubules close to the pole (Burbank et al., 2007).

In fact, dynein–dynactin might take advantage of the additional activity of Eg5 as a microtubule cross-linking agent that might provide part of the force required to clamp microtubules together close to the poles of the spindle. The efficiency of pole focusing by dynein–dynactin and spindle stability would in this scenario also depend on the local concentration of Eg5, which in turn would depend on the interaction of Eg5 with the dynein–dynactin complex. An assisting role for pole focusing by Eg5 is supported by the observations that isolated half spindles in uncycled cytostatic factor (CSF) extract have broader poles after inhibition or depletion of Eg5 (Sawin et al., 1992) and that, although microtubule asters with a central pole still form in Eg5-depleted mitotic mammalian cell extracts, these poles are less well focused than in asters with active Eg5 (Gaglio et al., 1996). The reported fragility of spindles formed after double inhibition of both dynein–dynactin and Eg5 (Mitchison et al., 2005) might also be, at least in part, a consequence of the lacking microtubule clamping activity by Eg5. Thus, spindle pole defects observed after removal of dynein–dynactin from the pole region may therefore not only be a consequence of lacking dynein activity per se, but could also, in part, be a consequence of the drastic reduction of the amount of Eg5 in the spindle toward the spindle poles.

In summary, we propose that in the *X. laevis* egg extract metaphase spindle, the function of Eg5 varies according to its position. In this model, Eg5 drives microtubule flux in the spindle center, where it acts largely independently of dynein–dynactin. Outside the spindle center, Eg5 is transported by dynein–dynactin and contributes to stabilizing spindle poles. What could be the origin of the positional dependence of the behavior of Eg5 in the metaphase spindle? In the simplest scenario, differences in microtubule organization along the spindle axis might affect the interaction between Eg5 and dynein–dynactin purely based on different mechanical constraints at different positions. Interestingly, a spatial variation of the roles of the Eg5 homologue Klp61F depending on the organization of the microtubules in the spindle was also discussed for *Drosophila melanogaster* embryo spindles (Sharp et al., 1999a). More complicated scenarios might involve additional position-dependent biochemical regulation. For example, the dynactin component $p150^{Glued}$ has been reported to interact with Eg5 in a Cdk1 phosphorylation–dependent manner in vitro (Blangy et al., 1997). Together with the observation that cyclin B accumulates at spindle poles (Hagting et al., 1998), Cdk1/cyclin B might promote the interaction of Eg5 with dynein–dynactin toward the poles of spindles.

In conclusion, our data support a model in which the motor Eg5 has spatially differentiated roles for spindle assembly and maintenance. We also showed, by using Eg5 as an example of an important spindle component, that internal spindle dynamics correlate with spindle morphology. This illustrates the importance of the interplay between kinetics and structure in self-organizing systems. In the future, it will be important to measure also the movements of other spindle motors to gain a more dynamic picture of their contribution to spindle self organization.

Materials and methods

Cloning

The complete reading frame of Eg5 (corresponding to amino acids 1–1,067; a gift of C.E. Walczak, Indiana University, Bloomington, IN) was PCR amplified, introducing a C-terminal pentaglycine linker, and inserted (NotI and XhoI) into pFastBacHTa (Invitrogen). To generate expression vectors for Eg5 with a C-terminal GFP or paGFP, a PCR-amplified, SalI–XhoI-digested sequence of enhanced GFP (Clontech Laboratories, Inc.) or paGFP (a gift of J. Lippincott-Schwartz, National Institutes of Health, Bethesda, MD; Patterson and Lippincott-Schwartz, 2002) was inserted into the XhoI site at the 3′ end of the pentaglycine linker sequence in pFastBacHTa carrying the Eg5 sequence, generating Eg5-GFP and Eg5-paGFP, respectively. The vector for expression of Eg5 with its last 76 amino acids replaced by paGFP (Eg5ΔC-paGFP) was constructed by adding an N-terminal pentaglycine linker sequence to paGFP by PCR amplification followed by inserting (XbaI–XhoI) the amplified fragment into the pFastBacHTa plasmid carrying the Eg5 sequence at the internal restriction site XbaI within the Eg5 sequence. A sequence corresponding to amino acids 174–505 that are predicted to form the first coiled coil (cc1; Quintyne et al., 1999) of *X. laevis* $p150^{Glued}$ was amplified from a p150 *X. laevis* cDNA plasmid (RZPD) and inserted (EcoRI–XhoI) into pGEX-6P-1 (GE Healthcare).

Protein purifications

Full-length Eg5 without GFP and fluorescent Eg5 constructs were expressed in Sf9 insect cells using the Bac-to-Bac baculovirus system (Invitrogen). Cells from a 350-ml culture were harvested 72 h after infection, suspended in 3.5 ml of lysis buffer (50 mM KP_i, pH 8.0, 250 mM KCl, 10 mM imidazole, 0.5 mM MgATP, 0.1% Triton X100, 5 mM mercaptoethanol [ME], and complete EDTA-free protease inhibitors [PI]; Roche) and frozen in liquid nitrogen. Thawed cells were lysed on ice, and the clarified lysate was loaded onto 3 ml of Talon metal affinity resin (Clontech Laboratories, Inc.) equilibrated with lysis buffer. The column was washed with 100 ml of wash buffer (50 mM KP_i, pH 8.0, 250 mM KCl, 10 mM imidazole, 0.1 mM MgATP, 10% glycerol, 5 mM ME, and PI), then with 30 ml wash buffer containing additional 10 mM imidazole, and the protein was finally eluted with a gradient of 20–250 mM imidazole in elution buffer (50 mM KP_i, pH 7.0, 150 mM KCl, 0.1 mM MgATP, 10% glycerol, 5 mM ME, and PI). Eluted Eg5 was dialyzed against dialysis buffer (50 mM imidazole, pH 7.0, 50 mM KCl, 0.5 mM EGTA, 10% [wt/vol] sucrose, and 10 mM ME), and frozen at a final concentration of 1 mg/ml in liquid ethane and stored in liquid nitrogen. Eg5 concentrations were determined by a Bradford assay, and molarities refer to Eg5 monomers, if not stated otherwise.

GST-cc1 was expressed in *E. coli* BL21-RIL (Stratagene) at 30°C for 3 h and was purified from clarified lysate using GST-bind resin (EMD) according to the manufacturer's instructions. The protein was dialyzed into 20 mM Tris-HCl, pH 7.5, 150 mM KCl, and 1 mM DTT, and cleaved at 4°C with GST-PreScission protease (European Molecular Biology Laboratory). Free GST and protease were removed with GST-Bind resin. cc1 was concentrated (Vivaspin; Sartorius) to a final concentration of 2.5 mg/ml, frozen, and stored at −80°C. p50 was purified as described previously (Wittmann and Hyman, 1999).

Tubulin was purified from porcine brain (Castoldi and Popov, 2003) and labeled with Alexa 568–succinimidyl ester, Cy5–succinimidyl ester, and biotin–XX–succinimidyl ester (all from Invitrogen) as described previously (Hyman et al., 1991). Polyclonal antibodies against Eg5 were a gift of J. Cahu (European Molecular Biology Laboratory, Heidelberg, Germany).

Microtubule pair sliding in buffer

Microtubules were polymerized from 40 µM tubulin supplemented either with 15 µM biotinylated tubulin and 5 µM Alexa 568–labeled tubulin (biotinylated; dimly labeled microtubules) or with 20 µM Alexa 568–labeled tubulin (or 10 µM Cy5-labeled tubulin; brightly labeled microtubules) in the presence of 1 mM GTP in BRB80 (80 mM Pipes, pH 6.8, 1 mM EGTA, and 1 mM $MgCl_2$) at 35°C for 30 min, pelleted by centrifugation at 20,000 *g* for 10 min, and resuspended in dialysis buffer supplemented with 20 µM paclitaxel (Sigma-Aldrich).

Flow chambers of ∼5 µl volume were constructed from one functionalized and one nonfunctionalized glass coverslip using double sticky tape (Tesa Tape) as a spacer. To generate functionalized glass, coverslips were covalently coated with biotin–polyethylene glycol (biotin-PEG) as described previously (Bieling et al., 2007). In brief, the glass was silanized, passivated with diamine-PEG (Lata and Piehler, 2005), and finally treated with N-hydroxysuccinimide–biotin.

Microtubules were immobilized on the biotin-PEG glass surface by applying the following sequence of solutions to the flow chamber: 4 chamber volumes of dialysis buffer, 4 volumes of 3 µM neutravidin (Invitrogen) in dialysis buffer, and 4 volumes of 0.4 µM biotinylated microtubules in dialysis buffer. Unattached microtubules were washed out by 10 volumes of assay buffer (50 mM imidazole, pH 7.0, 100 mM KCl, 0.5 mM EGTA, 10% sucrose, 10 mM mercaptoethanol, 0.1 mg/ml β casein, and 20 µM paclitaxel). 2 volumes of 0.2% pluronic F-127 (Sigma-Aldrich) in assay buffer were introduced into the chamber to block the nonfunctionalized cover glass followed by rinsing with 10 volumes of assay buffer B (assay buffer containing 1 µM MgATP). Eg5 was bound to the immobilized microtubules by adding 50 nM recombinant Eg5 in assay buffer B followed by a wash with 4 volumes of assay buffer B. The flow chamber was then incubated with 0.4 µM of brightly labeled or Cy5-labeled microtubules suspended in assay buffer B for 3 min, which allowed for microtubule pair formation. Finally, antiparallel microtubule sliding was initiated by introducing 2 volumes of assay buffer supplemented with 100 nM recombinant Eg5, 5 mM MgATP, and oxygen scavengers (8 mM glucose, 0.1 mg/ml glucose oxidase [Sigma-Aldrich], and 0.03 mg/ml catalase [Sigma-Aldrich]).

Single-color time-lapse fluorescence microscopy was performed at 25°C on a wide-field cell observer (AxioVision) with a 63× oil immersion objective and a camera (AxioCam MRm; all from Carl Zeiss, Inc.), using 5-s time intervals, and 300-ms exposure time. Dual-color time-lapse fluorescence imaging was performed on a confocal microscope (LSM 510; Carl Zeiss, Inc.) with 543- and 633-nm excitation lines, dual-band pass 560–615 and 700–800 nm for detection, a 63× oil immersion objective, and 5-s time intervals between image frames. Velocity distributions were generated from analyzing time–space plots (kymographs) of sliding microtubules created in ImageJ using the Kymograph plug-in (Seitz and Surrey, 2006). Mean velocities were obtained from Gaussian fits to the distributions.

Spindle assembly in *X. laevis* egg extracts

Nucleocytoplasmic extracts of unfertilized *X. laevis* eggs arrested in metaphase of meiosis II were prepared as described previously (Hannak and Heald, 2006), with minor modifications. Spindles were assembled in extract around purified *X. laevis* sperm nuclei after cycling the extract once through interphase back into metaphase (Hannak and Heald, 2006). Incubation of extract was performed at 22°C, and metaphase spindles were observed after 30 min.

For depletion/add-back experiments, Eg5 was immunodepleted from 50 µl extract by two successive rounds of 30-min incubations of the extract with 30 µl of protein A–Dynabeads (Invitrogen) saturated with polyclonal anti-Eg5 antibody. For control experiments, extract was treated in the same manner with protein A–Dynabeads saturated with an irrelevant IgG. Sperm nuclei, Alexa 568– or Cy5-labeled tubulin, and in some experiments, p50 (or dialysis buffer for controls), were then added to the immunodepleted extract. Spindles were then sent to interphase by addition of calcium. After a 1-h incubation at 22°C, recombinant Eg5, and, in some experiments, cc1, were added, and the extract was cycled back to mitosis by addition of depleted extract. Final concentrations were 0.3 µM of recombinant Eg5, 2 µM Cy5-tubulin, and 500 nuclei/µl, and in some experiments 23 µM p50 or 3.3 µM cc1.

Fluorescence imaging of fixed spindles

To prepare fixed spindles, they were centrifuged from 20 µl of extract through a glycerol cushion onto glass coverslips and then fixed in 4% formaldehyde as described previously (Hannak and Heald, 2006). DNA in fixed spindles was stained with 10 µg/ml Hoechst in PBS. The efficiency of bipolar spindle versus monoaster formation was evaluated by counting fixed structures. For detection of dynein or dynactin in wild-type spindles or in cc1- or p50-treated spindles, immunofluorescence of formaldehyde fixed spindles containing Alexa 568–labeled microtubules was performed. Coverslips were washed with 0.1 M glycin in TBS with Tween (TBST) to quench remnants of formaldehyde, blocked with 2% BSA in TBST, and incubated for 30 min with 11 µg/ml of a purified polyclonal antibody raised against a C-terminal fragment of the dynein heavy chain corresponding to amino acids 4,179–4,415 (a gift of S. Kandels-Lewis and S. Rybina; European Molecular Biology Laboratory, Heidelberg, Germany) or with 4 ng/ml of a mouse monoclonal antibody raised against $p150^{Glued}$ (BD Biosciences). After incubation with primary antibody, coverslips were washed in TBST containing 10 µg/ml Hoechst and incubated for 30 min with 10 µg/ml of secondary antibody fused to Alexa Fluor 488 (Invitrogen), and finally washed in TBST. Images were taken with a confocal LSM 510 microscope with laser lines of 405, 488, 543, and 633 nm and a 63× oil immersion objective lens.

Pull-down assay

100 µl of magnetic protein A beads (Invitrogen) were saturated with polyclonal rabbit anti-Eg5 generated as described previously (Sawin et al., 1992), 100 µl of magnetic protein G beads (Invitrogen) were saturated with monoclonal mouse anti-$p150^{Glued}$ (BD Biosciences), or beads were saturated for controls with an irrelevant rabbit IgG antibody according to the manufacturer's instructions; beads were then washed with CSF extract buffer (Hannak and Heald, 2006). Part of a CSF arrested mitotic *X. laevis* egg extract was incubated with cc1 at a final concentration of 3.3 µM and nocodazole at a final concentration of 40 µM for 45 min on ice. 25 µl of extract with or without cc1 was mixed with 25 µl of antibody beads and incubated for 35 min at 22°C. The beads were then washed three times with 100 µl PBS and boiled in 50 µl SDS sample buffer, and finally removed. Each sample was analyzed by Western blotting. For the pull-down of p150, primary anti-Eg5 and anti-p150 antibodies were applied overnight at concentrations of 0.02 µg/ml and 0.5 µg/ml, respectively. For the pull-down of Eg5, primary anti-Eg5 and anti-p150 antibodies were applied for 1 h at concentrations of 0.45 µg/ml and 0.08 µg/ml, respectively. The secondary HRP antibody (Santa Cruz Biotechnology, Inc.) was used at a dilution of 1:5,000.

Imaging of the dynamics of Eg5 and tubulin in spindles

1.5 µl of extract with assembled spindles was placed gently between two glass coverslips, and spindles were observed for a maximum time period

of 5 min. The temperature was kept at 25°C. Photoactivation of Eg5 constructs fused to paGFP and photobleaching of Cy5-tubulin was performed by illuminating an elongated rectangular region of 3 × 40 µm, perpendicular to the pole-to-pole axis, simultaneously with the 405- and 633-nm light of a confocal microscope. The lowest possible laser powers sufficient for efficient photoactivation and photobleaching were used. In some control experiments, Eg5-paGFP was photoactivated without simultaneously photobleaching Cy5-tubulin. Time-lapse imaging of the fluorescence of photoactivated paGFP and of Cy5 was performed before and after photoactivation/photobleaching (LSM 510, 63× 1.2w NA immersion objective [Carl Zeiss, Inc.], 488- and 633-nm excitation lines, band pass 505–530 nm and long pass 650 nm for detection, pinhole of 3 µm, 8-s time intervals between image frames, 25.6-µs pixel time, and 512/97.5 × 512/97.5 pixel/µm image size). We analyzed the dynamics of Eg5-paGFP in 19 spindles assembled in five different extracts, of Eg5ΔC-paGFP in six spindles, and of Cy5 microtubules in 16 spindles.

To test for the potential contribution of bleaching to the measurement of Eg5 turnover, we measured the time course of the fluorescence intensity of Cy5 tubulin in an area of the spindle where no tubulin bleach mark was set initially, and used a monoexponential fit to the data to determine the bleaching rate (Fig. S2 b, left). To test for the potential contribution of bleaching to the measurement of Eg5 turnover, we measured the time course of the GFP fluorescence intensity of Eg5-GFP in spindles reconstituted in extract in which native Eg5 was replaced by recombinant Eg5-GFP, and used a monoexponential fit to the data to determine the bleaching rate (Fig. S2 b, right). All microscope settings were identical to those used during a turnover measurement. In both cases, the bleaching rate was found to be negligible as compared with the measured turnover rates of microtubules and Eg5.

In control experiments, the speed of microtubule flux was also measured by fluorescent speckle microscopy (Waterman-Storer and Danuser, 2002). From a total of 11 spindles, we obtained an average speckle flux velocity of 1.9 ± 0.3 µm/min (Fig. S3), which is similar to previous studies (Sawin and Mitchison, 1991; Desai et al., 1998; Maddox et al., 2003). This flux velocity was not statistically different from our measured flux velocities obtained by photobleaching (Mann-Whitney *U* test: P = 0.0989, significance level 0.05). The spindles used for speckle microscopy were assembled in Eg5-depleted, cycled extract supplemented with 0.3 µM of recombinant Eg5-paGFP and 15 nM of Alexa 568–labeled tubulin. Time lapse imaging with a 500-ms exposure time and 2-s interval time, covering a time period of 2 min, was performed on a epifluorescence microscope (Axiovert 135 TV; Carl Zeiss, Inc.) equipped with a 100× 1.4 NA oil objective and a camera (Cool Snap HQ; Roper Scientific).

Data analysis

Fluorescence intensity profiles were extracted from time-lapse images of spindles (Fig. 2) using a self-written ImageJ plugin. To determine the velocities of the movement of Eg5 and of microtubules in the spindle, the maxima of inverted intensity difference profiles of Cy5 microtubules and of intensity profiles of photoactivated Eg5-paGFP were obtained from Gaussian fits to the peaks and plotted as a function of time. A regression analysis yielded the velocities. To determine the turnover of Eg5 and tubulin from fluorescence decays and recoveries after photoactivation and photobleaching at the various spindle positions, we first determined the range within which a given fluorescence peak was observed during the entire time lapse. The integrated areas under the profiles within this range were then plotted against time. This means that we followed the entire pool of photobleached tubulin or photoactivated Eg5 during the time course of the experiment. The measured turnover as defined here was therefore not affected by movement but was exclusively a consequence of binding/unbinding to/from the spindle structure. A potential contribution from bleaching could be neglected when analyzing the decays and recoveries (Fig. S2 b). Half-lives of turnover were determined from monoexponential fits to the data obtained during the first 2 min using $\tau_{1/2} = \ln 2/k$, with k being the time constants of the fluorescence decays and recoveries. The monoexponential fit to the data measured within the first 2 min after photoactivation or photobleaching resulted also in the detection of a "residual" pool of Eg5 and tubulin that does not turn over with monoexponential kinetics. This pool represents molecules that turn over more slowly, as was observed when the period of observation was extended to 5 min. This slower-turnover residual pool might be a consequence of rebinding events in the large spindle before the observed molecules leave the detection volume by diffusion. Because we always followed the entire photoactivated and photobleached population of molecules for the analysis of the turnover, this residual pool does not imply a "static" pool.

Online supplemental material

Fig. S1 shows that purified Eg5 fused to paGFP rescues spindle formation in egg extract immunodepleted from native Eg5. Fig. S2 a shows an example of a photoactivation/photobleaching experiment in an egg extract spindle. Fig. S2 b shows that there is no contribution of bleaching to the turnover during time-lapse imaging of fluorescently labeled tubulin and Eg5 in the spindle. Fig. S3 shows a control experiment in which microtubule flux was measured by speckle microscopy. Fig. S4 illustrates the localization of dynein and dynactin in fixed spindles. Fig. S5 presents the analysis of a truncated Eg5 construct lacking a C-terminal part of its sequence. Videos 1 and 2 show a time-lapse fluorescence video of photoactivated Eg5-paGFP and of Cy5 microtubules after photobleaching, respectively. Video 3 is an overlay of Video 1 and 2. Online supplemental material is available at http://www.jcb.org/cgi/content/full/jcb.200801125/DC1.

We thank Mathias Utz for technical assistance; Ivo Telley for help with data analysis; Timo Zimmermann, Arne Seitz, Joel Beaudouin, and Jan Ellenberg for help with confocal microscopy; Jacob Piehler for help with surface chemistry on glass; Henry Schek, Iva Kronja, and Thomas Mayer for suggestions; and Kresimir Crnokic from the animal facility for taking care of the frogs.

M. Uteng acknowledges support from the Norwegian Research Council (NFR; grant 159989/V40), C. Hentrich from the European Union Marie Curie Research Training Network "Spindle Dynamics" (grant 512348) and T. Surrey and P. Bieling from the German Research Foundation (DFG; grant SU 175/4-1,2).

Submitted: 22 January 2008
Accepted: 23 July 2008

References

Bieling, P., L. Laan, H. Schek, E.L. Munteanu, L. Sandblad, M. Dogterom, D. Brunner, and T. Surrey. 2007. Reconstitution of a microtubule plus-end tracking system in vitro. *Nature.* 450:1100–1105.

Blangy, A., H.A. Lane, P. d'Herin, M. Harper, M. Kress, and E.A. Nigg. 1995. Phosphorylation by p34cdc2 regulates spindle association of human Eg5, a kinesin-related motor essential for bipolar spindle formation in vivo. *Cell.* 83:1159–1169.

Blangy, A., L. Arnaud, and E.A. Nigg. 1997. Phosphorylation by p34cdc2 protein kinase regulates binding of the kinesin-related motor HsEg5 to the dynactin subunit p150. *J. Biol. Chem.* 272:19418–19424.

Burbank, K.S., A.C. Groen, Z.E. Perlman, D.S. Fisher, and T.J. Mitchison. 2006. A new method reveals microtubule minus ends throughout the meiotic spindle. *J. Cell Biol.* 175:369–375.

Burbank, K.S., T.J. Mitchison, and D.S. Fisher. 2007. Slide-and-cluster models for spindle assembly. *Curr. Biol.* 17:1373–1383.

Cameron, L.A., G. Yang, D. Cimini, J.C. Canman, O. Kisurina-Evgenieva, A. Khodjakov, G. Danuser, and E.D. Salmon. 2006. Kinesin 5–independent poleward flux of kinetochore microtubules in PtK1 cells. *J. Cell Biol.* 173:173–179.

Castoldi, M., and A.V. Popov. 2003. Purification of brain tubulin through two cycles of polymerization-depolymerization in a high-molarity buffer. *Protein Expr. Purif.* 32:83–88.

Cole, D.G., W.M. Saxton, K.B. Sheehan, and J.M. Scholey. 1994. A "slow" homotetrameric kinesin-related motor protein purified from *Drosophila* embryos. *J. Biol. Chem.* 269:22913–22916.

Cross, R.A. 2004. The kinetic mechanism of kinesin. *Trends Biochem. Sci.* 29:301–309.

Desai, A., P.S. Maddox, T.J. Mitchison, and E.D. Salmon. 1998. Anaphase A chromosome movement and poleward spindle microtubule flux occur At similar rates in *Xenopus* extract spindles. *J. Cell Biol.* 141:703–713.

Ding, R., K.L. McDonald, and J.R. McIntosh. 1993. Three-dimensional reconstruction and analysis of mitotic spindles from the yeast, *Schizosaccharomyces pombe*. *J. Cell Biol.* 120:141–151.

Gadde, S., and R. Heald. 2004. Mechanisms and molecules of the mitotic spindle. *Curr. Biol.* 14:R797–R805.

Gaetz, J., and T.M. Kapoor. 2004. Dynein/dynactin regulate metaphase spindle length by targeting depolymerizing activities to spindle poles. *J. Cell Biol.* 166:465–471.

Gaglio, T., A. Saredi, J.B. Bingham, M.J. Hasbani, S.R. Gill, T.A. Schroer, and D.A. Compton. 1996. Opposing motor activities are required for the organization of the mammalian mitotic spindle pole. *J. Cell Biol.* 135:399–414.

Goshima, G., and R.D. Vale. 2003. The roles of microtubule-based motor proteins in mitosis: comprehensive RNAi analysis in the *Drosophila* S2 cell line. *J. Cell Biol.* 162:1003–1016.

Hagan, I., and M. Yanagida. 1992. Kinesin-related cut7 protein associates with mitotic and meiotic spindles in fission yeast. *Nature.* 356:74–76.

Hagting, A., C. Karlsson, P. Clute, M. Jackman, and J. Pines. 1998. MPF localization is controlled by nuclear export. *EMBO J.* 17:4127–4138.

Hannak, E., and R. Heald. 2006. Investigating mitotic spindle assembly and function in vitro using *Xenopus laevis* egg extracts. *Nat. Protoc.* 1:2305–2314.

Heald, R., R. Tournebize, A. Habermann, E. Karsenti, and A. Hyman. 1997. Spindle assembly in *Xenopus* egg extracts: respective roles of centrosomes and microtubule self-organization. *J. Cell Biol.* 138:615–628.

Hildebrandt, E.R., and M.A. Hoyt. 2000. Mitotic motors in *Saccharomyces cerevisiae*. *Biochim. Biophys. Acta.* 1496:99–116.

Hyman, A., D. Drechsel, D. Kellogg, S. Salser, K. Sawin, P. Steffen, L. Wordeman, and T. Mitchison. 1991. Preparation of modified tubulins. *Methods Enzymol.* 196:478–485.

Kapitein, L.C., E.J. Peterman, B.H. Kwok, J.H. Kim, T.M. Kapoor, and C.F. Schmidt. 2005. The bipolar mitotic kinesin Eg5 moves on both microtubules that it crosslinks. *Nature.* 435:114–118.

Kapoor, T.M., and T.J. Mitchison. 2001. Eg5 is static in bipolar spindles relative to tubulin: evidence for a static spindle matrix. *J. Cell Biol.* 154:1125–1133.

Kashina, A.S., R.J. Baskin, D.G. Cole, K.P. Wedaman, W.M. Saxton, and J.M. Scholey. 1996. A bipolar kinesin. *Nature.* 379:270–272.

King, S.J., and T.A. Schroer. 2000. Dynactin increases the processivity of the cytoplasmic dynein motor. *Nat. Cell Biol.* 2:20–24.

King, S.J., C.L. Brown, K.C. Maier, N.J. Quintyne, and T.A. Schroer. 2003. Analysis of the dynein-dynactin interaction in vitro and in vivo. *Mol. Biol. Cell.* 14:5089–5097.

Lata, S., and J. Piehler. 2005. Stable and functional immobilization of histidine-tagged proteins via multivalent chelator headgroups on a molecular poly(ethylene glycol) brush. *Anal. Chem.* 77:1096–1105.

Lippincott-Schwartz, J., N. Altan-Bonnet, and G.H. Patterson. 2003. Photobleaching and photoactivation: following protein dynamics in living cells. *Nat. Cell Biol.* (Suppl):S7–S14.

Maddox, P., A. Straight, P. Coughlin, T.J. Mitchison, and E.D. Salmon. 2003. Direct observation of microtubule dynamics at kinetochores in *Xenopus* extract spindles: implications for spindle mechanics. *J. Cell Biol.* 162:377–382.

Mastronarde, D.N., K.L. McDonald, R. Ding, and J.R. McIntosh. 1993. Interpolar spindle microtubules in PTK cells. *J. Cell Biol.* 123:1475–1489.

Mayer, T.U., T.M. Kapoor, S.J. Haggarty, R.W. King, S.L. Schreiber, and T.J. Mitchison. 1999. Small molecule inhibitor of mitotic spindle bipolarity identified in a phenotype-based screen. *Science.* 286:971–974.

McIntosh, J.R., and U. Euteneuer. 1984. Tubulin hooks as probes for microtubule polarity: an analysis of the method and an evaluation of data on microtubule polarity in the mitotic spindle. *J. Cell Biol.* 98:525–533.

Melkonian, K.A., K.C. Maier, J.E. Godfrey, M. Rodgers, and T.A. Schroer. 2007. Mechanism of dynamitin-mediated disruption of dynactin. *J. Biol. Chem.* 282:19355–19364.

Miki, H., Y. Okada, and N. Hirokawa. 2005. Analysis of the kinesin superfamily: insights into structure and function. *Trends Cell Biol.* 15:467–476.

Mitchison, T., and M. Kirschner. 1984. Dynamic instability of microtubule growth. *Nature.* 312:237–242.

Mitchison, T.J., P. Maddox, J. Gaetz, A. Groen, M. Shirasu, A. Desai, E.D. Salmon, and T.M. Kapoor. 2005. Roles of polymerization dynamics, opposed motors, and a tensile element in governing the length of *Xenopus* extract meiotic spindles. *Mol. Biol. Cell.* 16:3064–3076.

Miyamoto, D.T., Z.E. Perlman, K.S. Burbank, A.C. Groen, and T.J. Mitchison. 2004. The kinesin Eg5 drives poleward microtubule flux in *Xenopus laevis* egg extract spindles. *J. Cell Biol.* 167:813–818.

Oiwa, K., and H. Sakakibara. 2005. Recent progress in dynein structure and mechanism. *Curr. Opin. Cell Biol.* 17:98–103.

Patterson, G.H., and J. Lippincott-Schwartz. 2002. A photoactivatable GFP for selective photolabeling of proteins and cells. *Science.* 297:1873–1877.

Quintyne, N.J., S.R. Gill, D.M. Eckley, C.L. Crego, D.A. Compton, and T.A. Schroer. 1999. Dynactin is required for microtubule anchoring at centrosomes. *J. Cell Biol.* 147:321–334.

Sawin, K.E., and T.J. Mitchison. 1991. Poleward microtubule flux mitotic spindles assembled in vitro. *J. Cell Biol.* 112:941–954.

Sawin, K.E., K. LeGuellec, M. Philippe, and T.J. Mitchison. 1992. Mitotic spindle organization by a plus-end-directed microtubule motor. *Nature.* 359:540–543.

Schroer, T.A. 2004. Dynactin. *Annu. Rev. Cell Dev. Biol.* 20:759–779.

Seitz, A., and T. Surrey. 2006. Processive movement of single kinesins on crowded microtubules visualized using quantum dots. *EMBO J.* 25:267–277.

Sharp, D.J., K.L. McDonald, H.M. Brown, H.J. Matthies, C. Walczak, R.D. Vale, T.J. Mitchison, and J.M. Scholey. 1999a. The bipolar kinesin, KLP61F, cross-links microtubules within interpolar microtubule bundles of *Drosophila* embryonic mitotic spindles. *J. Cell Biol.* 144:125–138.

Sharp, D.J., K.R. Yu, J.C. Sisson, W. Sullivan, and J.M. Scholey. 1999b. Antagonistic microtubule-sliding motors position mitotic centrosomes in *Drosophila* early embryos. *Nat. Cell Biol.* 1:51–54.

Sharp, D.J., H.M. Brown, M. Kwon, G.C. Rogers, G. Holland, and J.M. Scholey. 2000. Functional coordination of three mitotic motors in *Drosophila* embryos. *Mol. Biol. Cell.* 11:241–253.

Sprague, B.L., and J.G. McNally. 2005. FRAP analysis of binding: proper and fitting. *Trends Cell Biol.* 15:84–91.

Telzer, B.R., and L.T. Haimo. 1981. Decoration of spindle microtubules with Dynein: evidence for uniform polarity. *J. Cell Biol.* 89:373–378.

Tirnauer, J.S., E.D. Salmon, and T.J. Mitchison. 2004. Microtubule plus-end dynamics in *Xenopus* egg extract spindles. *Mol. Biol. Cell.* 15:1776–1784.

Vale, R.D., and R.A. Milligan. 2000. The way things move: looking under the hood of molecular motor proteins. *Science.* 288:88–95.

Valentine, M.T., P.M. Fordyce, T.C. Krzysiak, S.P. Gilbert, and S.M. Block. 2006. Individual dimers of the mitotic kinesin motor Eg5 step processively and support substantial loads in vitro. *Nat. Cell Biol.* 8:470–476.

Walczak, C.E., I. Vernos, T.J. Mitchison, E. Karsenti, and R. Heald. 1998. A model for the proposed roles of different microtubule-based motor proteins in establishing spindle bipolarity. *Curr. Biol.* 8:903–913.

Waterman-Storer, C., A. Desai, and E.D. Salmon. 1999. Fluorescent speckle microscopy of spindle microtubule assembly and motility in living cells. *Methods Cell Biol.* 61:155–173.

Waterman-Storer, C.M., and G. Danuser. 2002. New directions for fluorescent speckle microscopy. *Curr. Biol.* 12:R633–R640.

Wittmann, T., and T. Hyman. 1999. Recombinant p50/dynamitin as a tool to examine the role of dynactin in intracellular processes. *Methods Cell Biol.* 61:137–143.

Wittmann, T., A. Hyman, and A. Desai. 2001. The spindle: a dynamic assembly of microtubules and motors. *Nat. Cell Biol.* 3:E28–E34.

Yang, G., B.R. Houghtaling, J. Gaetz, J.Z. Liu, G. Danuser, and T.M. Kapoor. 2007. Architectural dynamics of the meiotic spindle revealed by single-fluorophore imaging. *Nat. Cell Biol.* 9:1233–1242.